Ibn Al-Haitham Journal for Pure and Applied Sciences
Journal homepage: jih.uobaghdad.edu.iq
PISSN: 1609-4042, EISSN: 2521-3407
IHJPAS. 2026; 39(2)

New Phenolic-Carbonyl Azo Ligand and its Binding Modes, Geometry Assignments and Thermal Behavior for Ligand and its Metal Complexes

Safaudeen Ali Hussain[1], and Enaam Ismail Yousif[2*]
[1,2]Department of Chemistry, College of Education for Pure Science (Ibn Al-Haitham), University of Baghdad, Baghdad, Iraq
*Corresponding Author

Received:21/November/2025
Accepted: 8/February/2026
Published: 20/April/2026
doi.org/10.30526/39.2.4332

Abstract

A fabricated Azo ligand (E)-1-[4-(3,4-dichloro-2-hydroxyphenyl) diazenyl] phenylethan-1-one was produced by a coupling reaction between diazonium salt made from *p*-aminoacetophenone and a basic solution of 2,3-dichlorophenol. The azo compound was used to form complexes with Cr(III), Co(II), Ni(II), and Cu(II) ions at a 2L:1M molar ratio in an alcoholic medium. The ligand and its complexes were characterized using a set of spectroscopic techniques to obtain chemical and structural information. Infrared with Fourier transformation; ultraviolet and visible; $^{1}H/^{13}C$ nuclear magnetic resonance; mass; thermal analysis and micro elemental analysis spectrometry, as well as molar conductivity. The results certified the chemical moiety and geometric fabrication. Azo dye acts as a bidentate ligand with phenol/hydroxy terminals. The finding was that Cr(III), Co(II), and Ni(II) complexes were characterized by a six-coordinate (distorted octahedral) geometry, whereas the Cu(II) complex had a tetrahedral structure. Thermal decomposition of the ligand and the selected complex was studied to assess stability upon heating and to determine the final residue.

Keywords: 4-Aminoacetophenone, Azo dye, 2,3-Dichlorophenol, Metal complexe.

1. Introduction

An aromatic compound with one or more azo (-N=N-) groups represents a very wide structural and functional diversity of organic compounds[1]. The azo moiety is characterized by SP2 hybridization, which enhances the delocalization of the electronic configuration in aromatic systems[2,3]. This configuration involved several substituents, such as carbonyl, hydroxyl (OH), and amine (NH_2) groups, that enhance coordination and chromophoric effects[4]. Utilized in coordination chemistry as effective ligands, they are very common, which is attributed to their ability to act as multidentate electron donors through nitrogen and oxygen, and the stability conferred on transition metals. Inorganic, analytical, and materials chemistry benefit significantly from azo dye complexes owing to their thermal stability, unique electronic transitions, and catalytic properties[5–7]. Azo compounds serve fields like medicine and biology very well. Inflammatory, antibacterial, and anticancer were the main applications of the azo compound because of its magnificent active formula[8–12]. Exclusive pigmentation and high selectivity enable them to serve as biological indicators, molecular sensors, and characterization tools for biochemical techniques[13,14]. Approximately 70 percent of trade colors are azo dyes, which have dominated the manufacture of plastics, fabrics, cosmetics, and inks[15–17]. Changeable color, chemical stability, and low cost make azo dye the first choice in many industries. This work focuses on the formation of a new azo dye from *p*-aminoacetophenone and 2,3-dichlorophenol, which is then used as a bidentate ligand to design metal complexes with Cr(III),

Co(II), Ni(II), and Cu(II). Spectroscopic techniques elucidate the compounds' structural characteristics, while thermal analysis provides insight into their thermal stability and degradation behavior. Despite the abundance of research on azo compounds in scientific libraries, their widespread use necessitates enriching scientific research by discovering new compounds that expand the base of raw materials used in their preparation. This study aims to expand the data on azo-metal interactions and their potential applications in chemical, biological, and industrial fields.

2. Materials and Methods

2.1. Materials and procedures for experimentation

The nuclear magnetic resonance (NMR) spectra of the ligand (^{1}H and ^{13}C) were recorded using a Bruker 300 and 75 MHz spectrometer. Samples were dissolved in DMSO-d6, with tetramethylsilane (TMS) serving as the internal standard. These measurements were conducted at the University of Tehran, Islamic Republic of Iran. Fourier-transform infrared (FTIR) spectra were obtained using an FTIR-600 spectrometer at the College of Science, University of Baghdad, covering the range of 4000–200 cm^{-1} with KBr/CsI_2 pellets. Positive ion electrospray ionization mass spectrometry (ESI-MS) was performed using a Sciex mass spectrometer at the University of Tehran. Melting points were determined using a Stuart SMP4 electrothermal apparatus in the Department of Chemistry, College of Education for Pure Science (Ibn Al-Haitham), University of Baghdad. UV-visible absorption spectra were recorded using a Shimadzu UV-160A spectrophotometer across the 200–1000 nm range. Measurements were carried out at room temperature using 10^{-3} mol/L solutions in DMF, placed in 1 cm quartz cuvettes, at the Department of Chemistry, College of Education for Pure Science (Ibn Al-Haitham), University of Baghdad. Electrical conductivity of DMF solutions was measured at concentrations ranging from 10^{-3} M using a Cyber Scan CON 510 digital conductivity meter (Eutech Instruments) at the Department of Chemistry, College of Education for Pure Science (Ibn Al-Haitham), University of Baghdad. Elemental analysis for carbon, hydrogen, and nitrogen was conducted using a Heraeus Vario EL analyzer, while metal content was determined via atomic absorption spectroscopy using a Shimadzu AA-7000 instrument at the Central Service Laboratory, University of Tehran. Chloride ion concentrations were assessed by potentiometric titration using a Metrohm 686 Titro processor and 665 Dosim unit at Ibn Sina Company, Ministry of Industry, Iraq. Magnetic susceptibility measurements were performed using a Johnson Matthey balance at the Department of Chemistry, College of Science, Al-Mustansiriyah University. Thermogravimetric and differential thermogravimetric analyses (TGA) were carried out using an SDT Q600 V20.9 Build 20 instrument at Beam Gostar Taban Laboratory, Islamic Republic of Iran.

2.2. Synthesis

2.2.1. Preparation of (E)-1-[4-(3,4-dichloro-2-hydroxyphenyl) diazenyl] phenylethan-1-one (HL)

The synthesis of the precursor was modified according to established protocols[18]. Initially, 1.35 g (10 mmol) of 4-aminoacetophenone was dissolved in a 20 mL mixture of ethanol and distilled water, to which 2 mL of 36% hydrochloric acid was added for acidification. The solution was agitated until clarity was achieved, then cooled to 0-5 °C. Subsequently, an aqueous solution of 0.69 g (10 mmol) of sodium nitrite was introduced dropwise while maintaining continuous agitation. The diazotization reaction was conducted in an ice bath for one hour. In a distinct container, 1.63 g (10 mmol) of 2,3-dichlorophenol was dissolved in 20 mL of ethanol, along with 0.8 g (20 mmol) of sodium hydroxide (NaOH). The alkaline solution was added incrementally to the diazonium salt solution while maintaining a low temperature. The mixture is still being agitated for another 2 hours, as shown in **Scheme 1**. The resulting solution was split, and 100 mL of water acidified with 2 mL of 36% HCl was added until a yellow precipitate was observed. Distilled water was used for washing, and the specimens were dried under fresh air.

Recrystallization was performed in hot ethanol, followed by drying over diethyl ether. The yield was 2.25g (73%); the melting point was 298 °C.

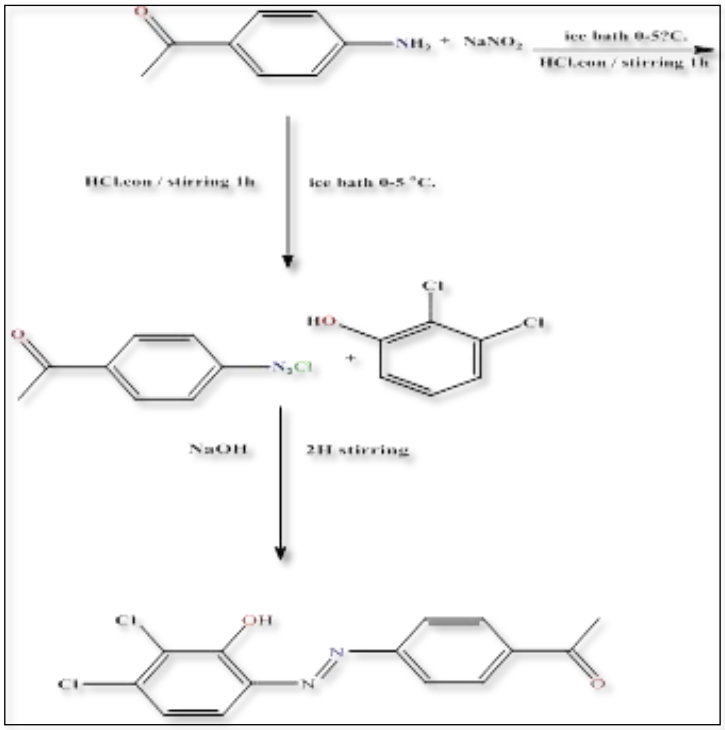

Scheme 1. General route for the synthesis of azo dye (HL)

2.2.2. Preparation of Cr (III) complexes

In this route, 0.618 g (2 mmol) of the fabricated ligand (HL) was dissolved in 10 mL of a solvent mixture of ethanol and DMF in a 3:1 volume ratio. About 10 mL of ethanolic solution containing 0.16 g (3 mmol) of potassium hydroxide (KOH) was added under continuous stirring. Following this, a solution of $CrCl_3.6H_2O$ (0.266 g, 1 mmol) in 5 mL of ethanol was gradually added to the reaction mixture. The mixture was then refluxed for 2 hrs. to promote complex formation. After the reaction was complete, the system was allowed to cool, and the resulting precipitate was collected by filtration, washed thoroughly with cold ethanol to eliminate residual reactants, and left to dry in air. The chromic complex was obtained as a solid with a yield of 0.492 g (63%) and a melting point above 300 °C.

2.2.3. Preparation of Co(II) complex

The synthesis approach followed a pathway similar to that used for the preparation of the chromic complex. The metal salt of $CoCl_2.6H_2O$ (0.237 g, 1 mmol) was used to make another complex. The cobalt complex was obtained as a solid with a yield of 0.469 g (57%) and a melting point above 300 °C.

2.2.4. Preparation of Ni(II) complex

The synthesis approach followed a pathway similar to that used for the preparation of the chromic complex. The metal salt $NiCl_2.6H_2O$ (0.237 g, 1 mmol) was used to prepare another complex. The nickel complex was obtained as a solid with a yield of 0.510 g (62%) and a melting point above 300 °C.

2.2.5. Preparation of Cu(II) complex

The synthesis approach followed a pathway similar to that used for the preparation of the chromic complex. The metal salt of $CuCl_2.2H_2O$ (0.170 g, 1 mmol) was used to make another complex. The copper complex was obtained as a solid in 62% yield (0.466 g) with a melting point above 300 °C. The synthetic pathway is depicted in **Scheme 2**, while **Table 1** summarizes the yields, colors, and melting points of the resulting complexes.

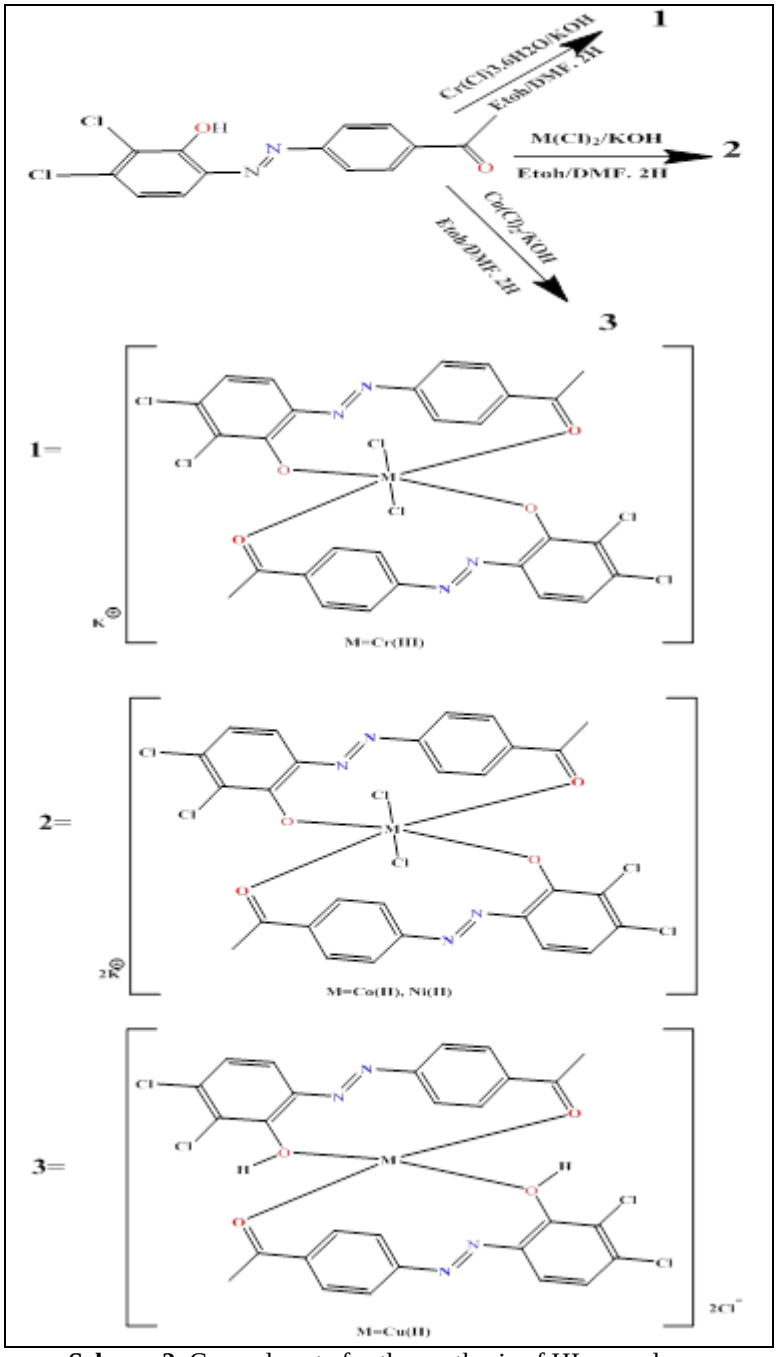

Scheme 2. General route for the synthesis of HL complexes

3. Results

The information on yields, colors, quantity of metal salts utilized, and m.p. for the resulting complexes is shown in **Table 1.** The proposed formula, molecular weight, and elemental microanalysis are shown in **Table 2.**

Table 1. Yield, colors and m.p. of compounds

Complexes	Yield (g)	Colors	m.p (ºC)	Yield (%)
HL	2.25	Fine yellow	298	73
$K[Cr(L)_2Cl_2]$	0.49	Greenish yellow	>300*	63
$K_2[Co(L)_2Cl_2]$	0.46	Brown	>300*	57
$K_2[Ni(L)_2Cl_2]$	0.51	Dark green	>300*	62
$[Cu(HL)_2]Cl_2$	0.46	Pale green	>300*	62

*=Decomposed.

Table 2. Micro-analysis and physical characteristics of compounds

Compound	Molecular formula	M.Wt	Microanalysis (calculated)% found				
			C	H	N	M	Cl
$K[Cr(L)_2Cl_2]$	$C_{28}H_{18}Cl_6CrKN_4O_4$	778.27	(43.21) 43.19	(2..33) 2.21	(7.20) 7.17	(11.70) 11.56	(27.33) 27.19
$K_2[Co(L)_2Cl_2]$	$C_{28}H_{18}Cl_6CoK_2N_4O_4$	824.30	(40.80) 40.73	(2.20) 2.03	(6.80) 6.33	(17.63) 17.13	(25.80) 25.57
K_2 $[Ni(L)_2Cl_2]$	$C_{28}H_{18}Cl_6NiK_2N_4O_4$	824.06	(40.81) 40.51	(2.20) 2.09	(6.80) 6.59	(16.61) 16.22	(25.81) 25.63
$[Cu(HL)_2]Cl_2$	$C_{28}H_{20}Cl_6CuN_4O_4$	752.74	(44.68) 44.55	(2.68) 2.39	(7.44) 7.01	(8.44) 8.32	(28.26) 28.13

3.1. FT-IR data

The FTIR of the ligand and its metal complexes displayed the following functional groups, which are shown in **Table 3** and **Figures 1-8**.

Table 3. The analysis of FT-IR for the most significant peaks (cm^{-1})

Complex	$(O-H)_{St}$	$\nu(C=O)_{ket}$	$\nu(C=C)_{aro.}$	$\nu(N=N)$	$\nu(M-O)_{car.}$ $\nu(M-O)_{ph.}$	$\nu(M-Cl)$
HL	3369	1678	1560	1492	-	-
$k[Cr(L)_2Cl_2]$	-	1667	1564	1493	606 559	295 260
$k_2[Co(L)_2Cl_2]$	-	1695	1558	1489	607 526	285 255
$k_2[Ni(L)_2Cl_2]$	-	1668	1581	1494	630 606	278 250
$[Cu(HL)_2]Cl_2$	3458	1699	1575	1489	642 606	-

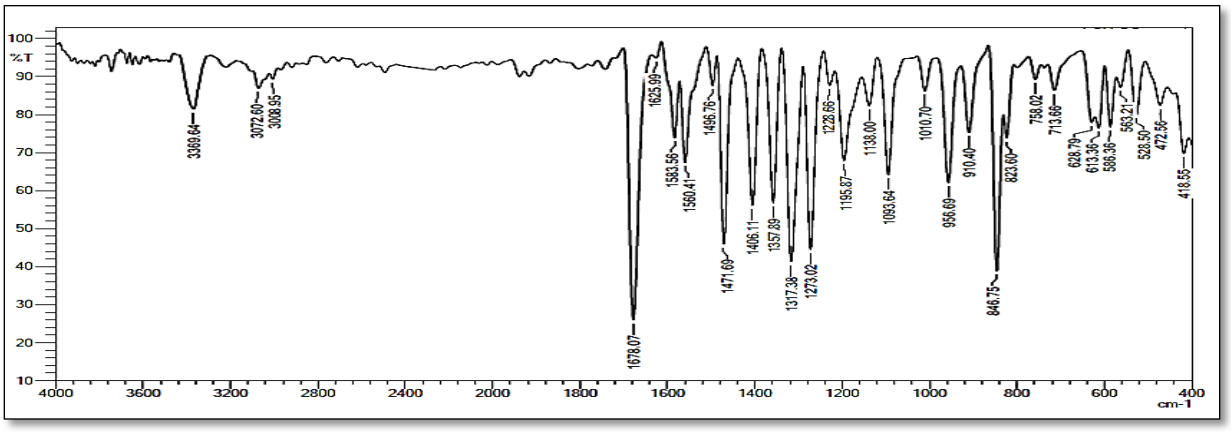

Figure 1. FTIR spectrum of ligand

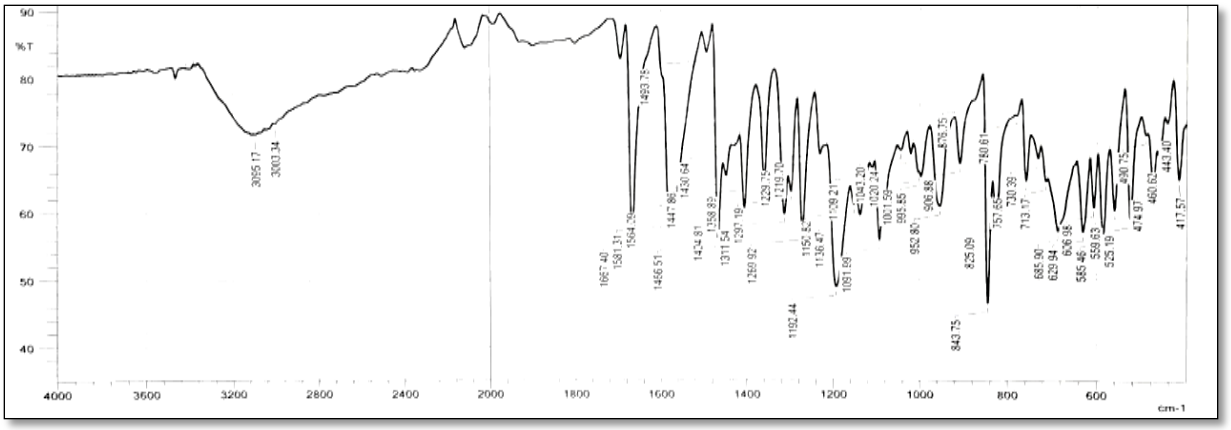

Figure 2. FTIR (400-4000 cm^{-1}) spectrum of Cr(III) complex

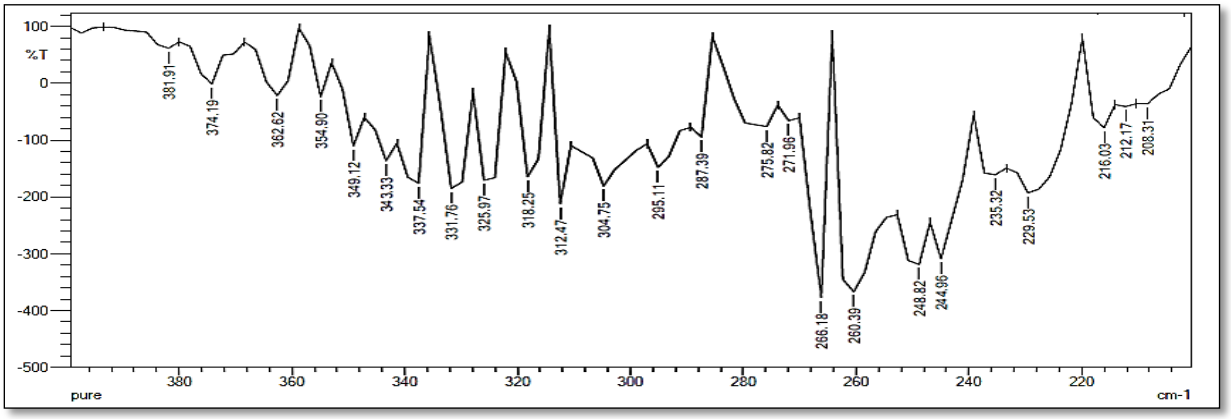

Figure 3. FTIR (200-400 cm^{-1}) spectrum of Cr(III) complex

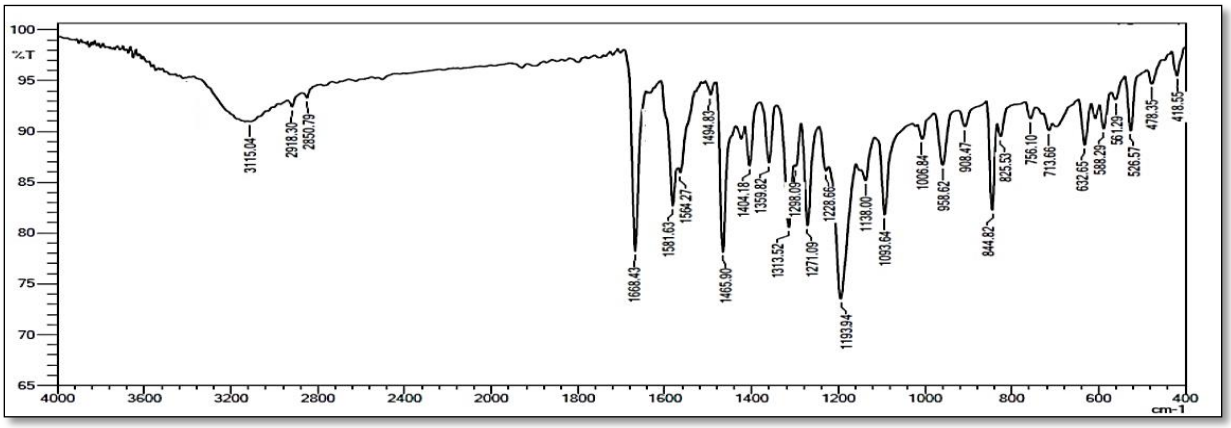

Figure 4. FTIR (400-4000 cm^{-1}) spectrum of Co(II) complex

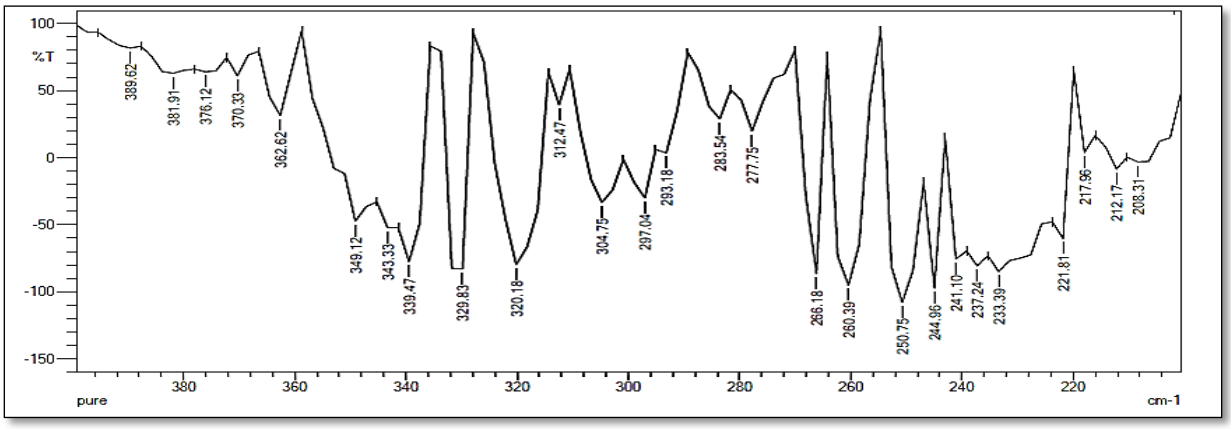

Figure 5. FTIR (200-400 cm^{-1}) spectrum of Co(II) complex

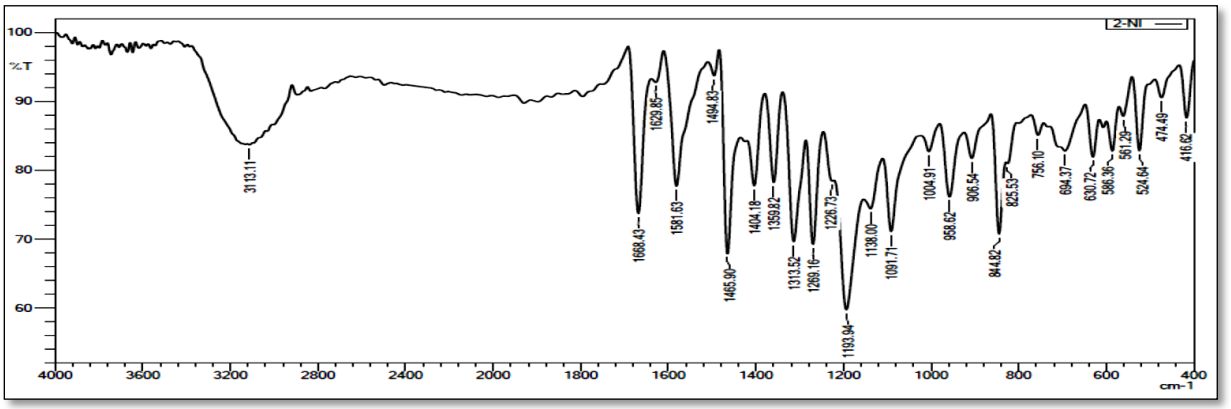

Figure 6. FTIR (400-4000 cm^{-1}) spectrum of Ni(II) complex

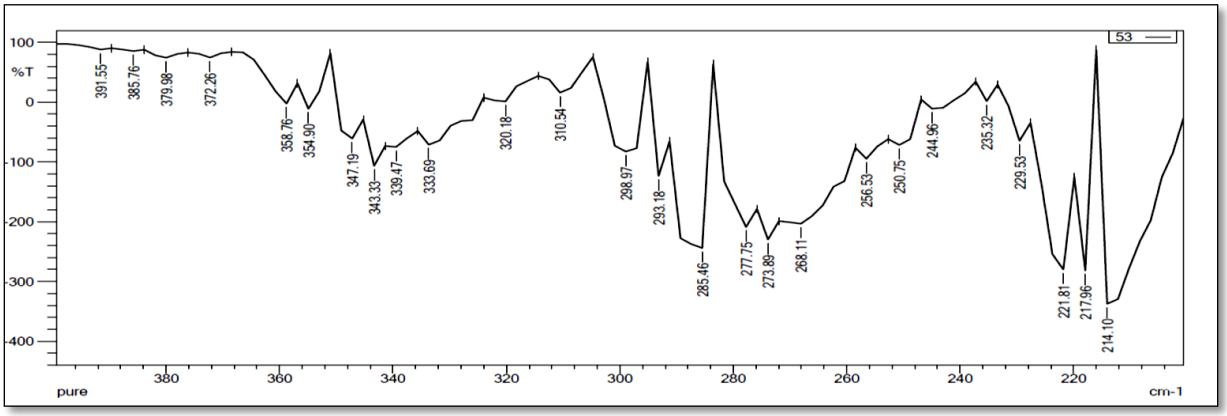

Figure 7. FTIR (200-400 cm^{-1}) spectrum of Ni(II) complex

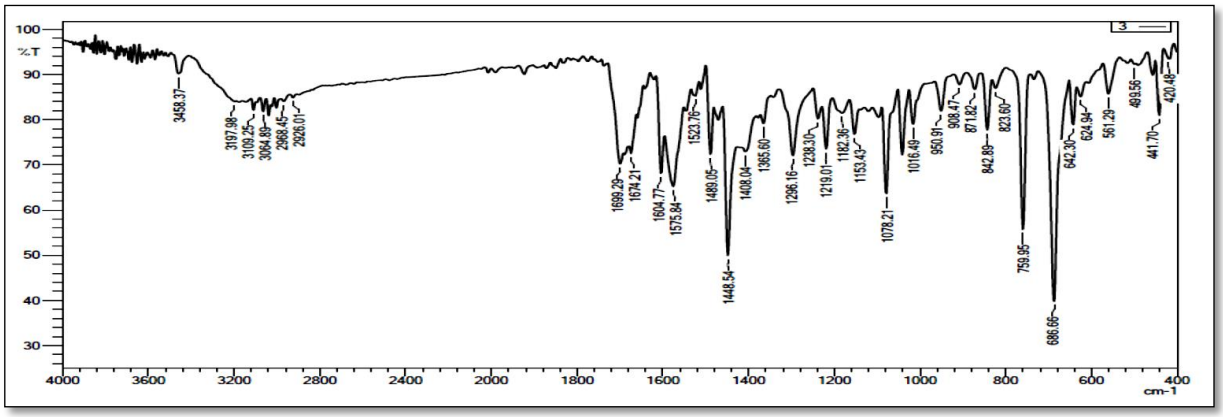

Figure 8. FTIR (200-400 cm^{-1}) spectrum of Cu (II) complex

3.2. NMR data

The ^{1}H NMR (300 MHz, DMSO6) was used to analyze HL in **Figure 9**. The spectrum showed two sets of bands: the first, the aromatic region, appeared around 6-9 ppm; the second, attributed to the aliphatic group, was assigned below 4 ppm, along with the solvent (DMSO6) and a trace of water. The ^{13}C NMR (75 MHz, DMSO6) was utilized for the analysis of HL in **Figure 10**. The spectrum illustrated two types of groups: aromatic, located in the downfield region above 100 ppm, and aliphatic, located below 40 ppm.

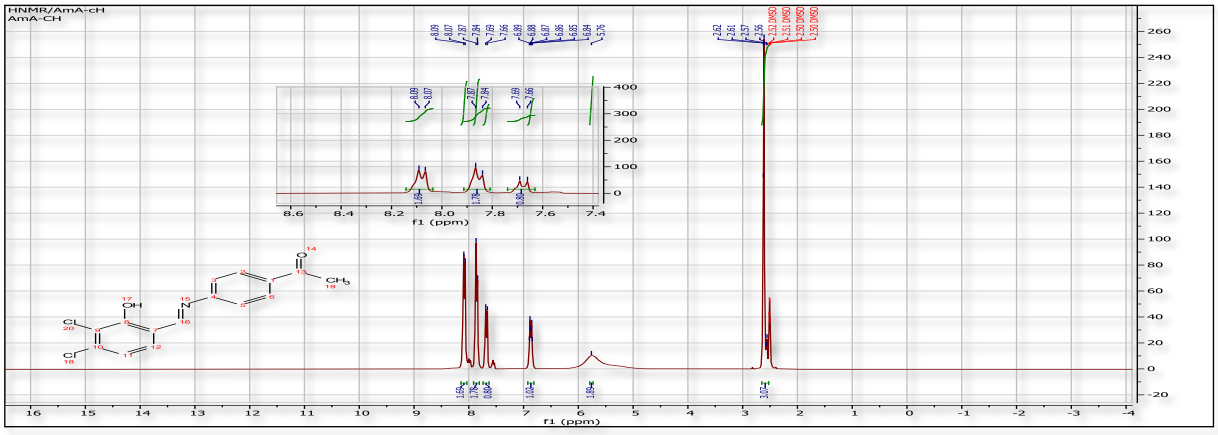

Figure 9. Spectrum of ^{1}H-NMR for the ligand

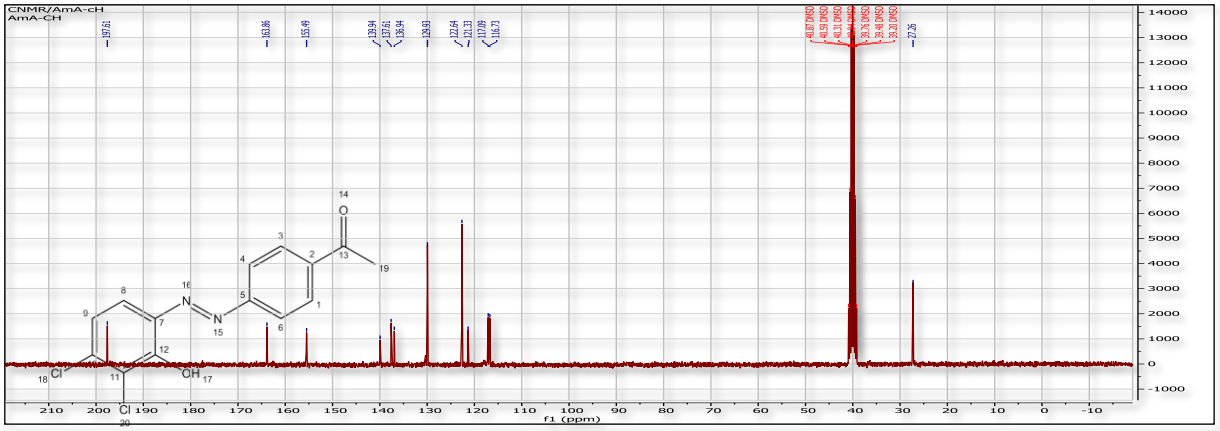

Figure 10. Spectrum ^{13}C-NMR spectra of the ligand

3.3. Mass spectrum

The mass of the HL was ascertained using the ESI-MS technique. The spectrum showed a mass-to-charge ratio of 332.85 g/mol, corresponding to $(M+Na)^+$, as shown in **Figure 11** and **Scheme 3**. For complexes, several other spectral and physical properties were relied upon in their diagnosis.

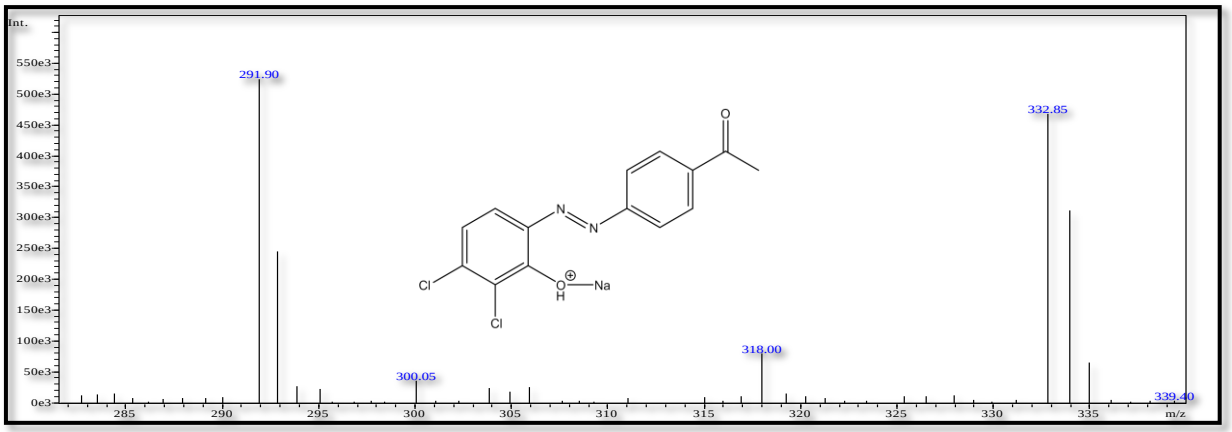

Figure 11. Mass spectrum of the ligand

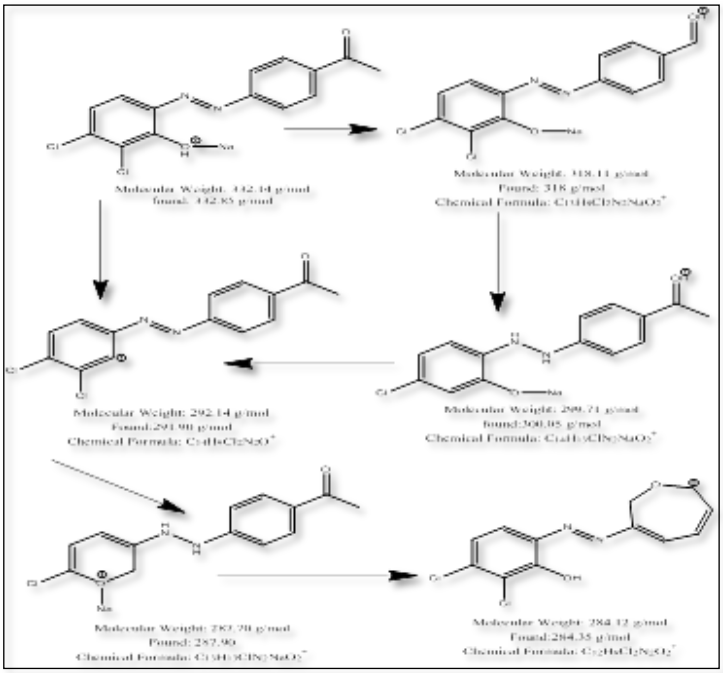

Scheme 3. The fragmentation pattern for the HL

3.4. Electronic spectra and magnetic moment

The electronic spectra, magnetic moments, and molar conductivities of the complexes are given in **Table 4**.

Table 4. The Uv-vis, molar conductivity and magnetic moment for complexes

Compounds	ʎnm	Molar extinction coefficient εmax (dm^3. mol^{-1} . cm^{-1})	Type of electron transition	Λm $S.cm^2$. $mole^{-1}$	μ_{eff}	Geometrical stricture
HL	267 363	1570 3700	$\pi \rightarrow \pi^*$ $n \rightarrow \pi^*$,	-	-	-
$k[Cr(L)_2Cl_2]$	268 520	68 77	Ligand field $^4A_2g \rightarrow {}^4T_1g^{(P)}$	43	2.91	Distorted octahedral
$k_2[Co(L)_2Cl_2]$	334 398 894	1903 1710 10	Ligand field C.T $^4T_1g^{(F)} \rightarrow {}^4T_2g^{(F)}$	80	3.66	Distorted octahedral
$k_2[Ni(L)_2Cl_2]$	269 353 657	1942 1960 40	Ligand field C.T $^3A_2g^{(F)} \rightarrow {}^3T_2g^{(F)}$	68	2.91	Distorted octahedra
$[Cu(HL)_2]Cl_2$	251 504	1030 290	Ligand field $^2B_1g \rightarrow {}^2A_2g$	74	1.88	tetrahedral

3.5. Thermal analysis

The TGA analysis of the ligand and the Cu(II) complex was performed. Thermos-cracking was shown in **Figures 12** and **13**.

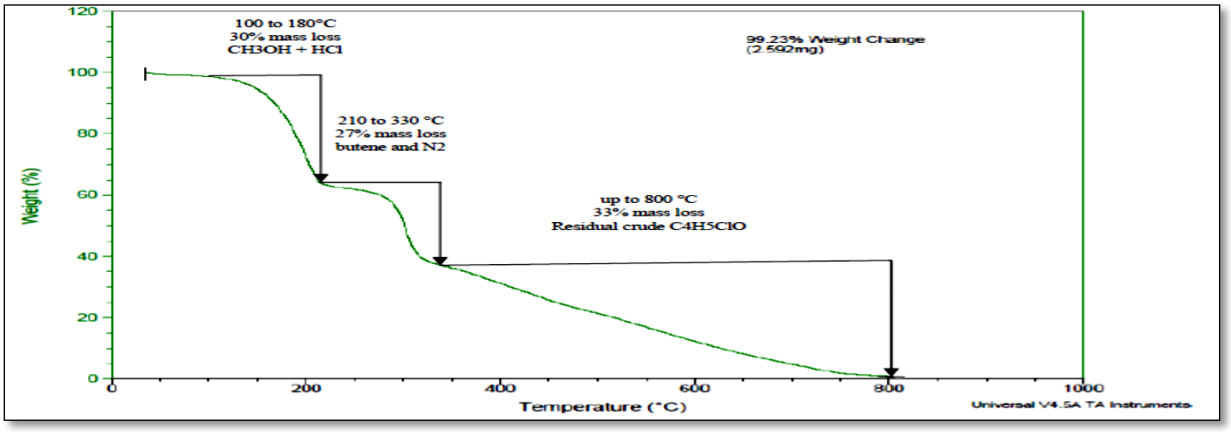

Figure 12. The thermal analysis curves of ligand in Ar atmosphere

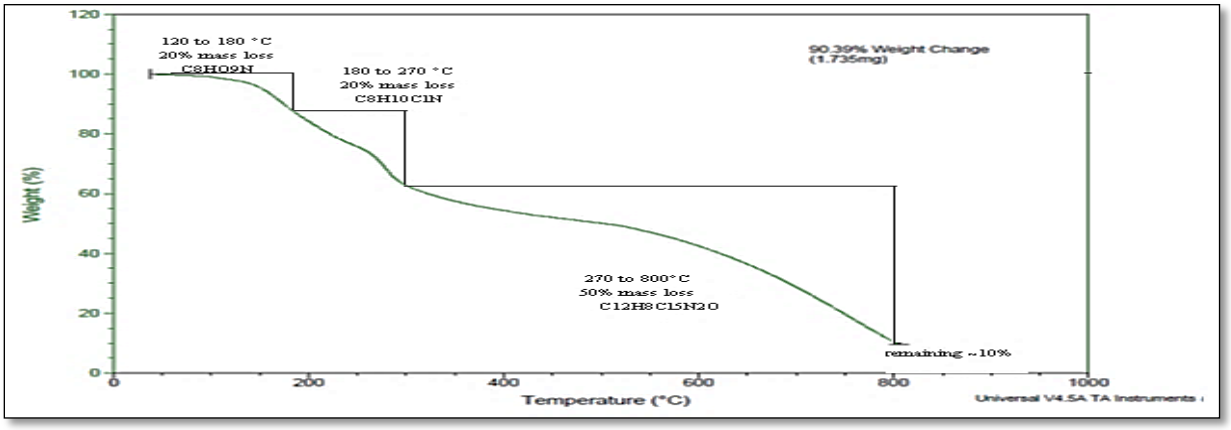

Figure 13. The thermal analysis curves of Cu(II) complex in Ar atmosphere

4. Discussion

A new azo dye, designated as (E)-1-[4-(3,4-dichloro-2-hydroxyphenyl) diazenyl] phenylethan-1-one, was synthesized through the diazotization of 4-aminoacetophenone followed

by its coupling with 2,3-dichlorophenol under alkaline conditions. The structure and properties of the dye were thoroughly characterized using various spectroscopic techniques, including FTIR, $^{1}H/^{13}C$ NMR, MS, and elemental analysis. Subsequently, metal complexes of the dye were prepared with Cr(III), Co(II), Ni(II), and Cu(II) ions using a 2:1 ligand-to-metal molar ratio in alcoholic media. These complexes were analyzed using FTIR, UV-Visible spectroscopy, molar conductivity measurements, and TGA analysis to evaluate their structural features and thermal stability. The results revealed that the azo dye acts as a bidentate ligand, coordinating through its phenolic and carbonyl oxygen atoms. The stereo shape of the designed complexes revolves around the metal ions: Cr(III), Co(II), and Ni(II) complexes, diagnosed as a distorted octahedral geometry. The Cu(II) complex is characterized by a tetrahedral shape. The heating evaluation demonstrated high thermal stability of the ligand and the selected complex during decomposition, with identifiable final residues. This result led to the suggestion that the fabricated dye and its metal complexes have potential applications in dyeing processes and catalytic systems, with physicochemical properties tunable by the selected metal center.

4.1. FT-IR and NMR data

The FTIR spectra of the designated azo dye HL ligand and coordination complexes were obtained. According to the results, the ligand exhibits frequencies that differ from those of the same area as the starting materials. The disappearance of the ($N–H_2$) stretching doublet at 3324 and 3394 cm^{-1} proved the involvement of the NH_2 group in the azo coupling reaction. A phenolic O–H stretching band was observed[18] at 3369 cm^{-1}. The azo–phenol tautomerism reflects a dynamic equilibrium between two structural forms of hydroxy azo compounds: the azo–phenol form (Ar–N=N–Ar'–OH) and the hydrazone–quinone form (Ar–NH–N=Ar'=O). This tautomeric transformation involves proton migration and π-electron rearrangement across the conjugated system[2]. An alkene (C–H) stretching band appeared at 3072 cm^{-1}, while saturated (C–H) stretching was detected around 3008 cm^{-1}. The ketonic carbonyl stretching band was identified[19] at 1678 cm^{-1}. The (C=C) stretching vibration was assigned at 1560 cm^{-1}. A new weak peak at 1492 cm^{-1} was attributed to the diazo group. Additional bands observed at 1406, 1357, and 1317 cm^{-1} were assigned to (O–H) bending, (C–O) stretching, and (C–N) stretching vibrations, respectively[20,21]. The FTIR spectra of the ligand with Cr (III), Co (II), Ni (II), and Cu (II) complexes were obtained. The carbonyl band, which pointed at 1678 shifted to1667;1668;1668;1668;1699 cm^{-1} for with Cr(III), Co(II), Ni(II), and Cu(II) complexes respectively. The phenolic peak at 3369 cm^{-1} loosened upon complexation for all complexes except the Cu (II)complex, which shifted to 3458 cm^{-1}. The azo group shifted to 1489 cm^{-1} for all complexes. New peaks were assigned as metal carbonyl oxide 606; 606; 607; 630; 642 cm^{-1} and metal phenolic oxide 559; 522; 526; 606; 606 cm^{-1} for Cr (III), Co (II), Ni (II), and Cu(II) complexes, respectively. The metal chloride bonds appeared at (295;266), (298;285), (277;260), (266; 293) cm^{-1} for Cr(III), Co(II) and Ni(II) complexes, respectively[21,22]. **Figures 1-8** represent the spectrum of the ligand and its complexes. The main IR spectrum data for the ligand and the complexes will be displayed in **Table 3**. The ^{1}H NMR (300 MHz, DMSO) was used to analyze HL in **Figure 9**. The doublet signal, which appeared at 8.08ppm (d, J = 3.0 Hz, 2H), could be attributed to two protons located at (C1; C3)-H. Another two protons, which belong to (C4; C6)-H, are fixed at 7.84 (d, J = 6.0 Hz, 2H). The two single proton assignments (C8; C9) were indicated by doublet bands at 7.68 (d, J = 9.2 Hz, 1H) and 6.87 (d, J = 9.5 Hz, 1H). The broad single band at around 5.76 ppm (s, 1H) is assigned to the phenolic proton. The exchangeable protons, such as those bonded to oxygen (-OH) or nitrogen (-NH), undergo rapid exchange in solution, which affects their detection, chemical shift, and peak shape[23–26]. These protons often appear as broad peaks, and their chemical shift can vary with solvent, hydrogen bonding, pH, and temperature[27,28]. The aliphatic region shows a high singlet at 2.61 ppm assigned to the methyl group (C19)-H. Finally, the protons of the solvent DMSO appeared at approximately 2.51 ppm. ^{13}C NMR (75 MHz, DMSO) was used to analyze HL. The carbonyl signal was

observed at a low field position of 197.61 ppm, while the phenolic carbon nuclei were fixed at 163.86 ppm[29]. The carbon atom associated with one of the azo nitrogen sides (C5) is designated as 155.49 ppm. The azo signals (C7) are situated at 139.94 ppm. 137.61;136.94 ppm correspond to (C10;C11) due to significant deshelling influenced by electron-withdrawing groups. The same chemical shifts for (C4,6 and C1,3) resulted in signals appearing at 129.93 and 122.64 ppm. The (C2; C9) frequencies were observed at 121.33 and 117.09 ppm, respectively. The final aromatic carbon nucleus (C8) is designated at 116.73 ppm. The aliphatic methyl carbon is situated at 27.26 ppm. The excess signals may be attributed to impurities that co-deposited with the compound. The DMSO solvent signal is now stabilized at around 39-40 ppm, as shown in **Figure 10**.

4.2. Mass spectrum

The mass of the HL was ascertained using the ESI-MS technique. The spectrum depicted a mass value of 332.85 g/mol, corresponding to $(M+Na)^+$, in contrast to the theoretical molar mass of 309.15 g/mol[30]. The presence of the group (M+Na)+ was anticipated based on the synthesis method, which incorporates NaOH as a catalyst and as a protective group for the phenolic hydroxide against oxidizing agents[31–33]. Additional fragment moieties observed in the spectrum (284.35; 287.90; 291.90; 300.05; 318.00 g/mol) may be ascribed to $C_{12}H_9Cl_2N_2O_2$+; $C_{13}H_{13}ClN_2NaO_2$+; $C_{14}H_9Cl_2N_2O$+; $C_{14}H_{13}ClN_2NaO_2$+; $C_{13}H_8Cl_2N_2NaO_2$+) potential configurations in **Figure 11.**

4.3. Electronic spectra and magnetic moment

The magnetic moment values and UV-visible spectral data for the synthesized complexes are summarized in **Table 4**. **Figures 12** and **13** represent the ligand spectrum and its complexes. The electronic spectra exhibited characteristic absorption bands in the range 200–300 nm, attributable to π→π* and n→π* transitions. Moreover, charge transfer transitions occurred in the 300−420 nm region due to ligand-to-metal or metal-to-ligand interactions[34,35]. The electron-transfer band of the Cr(III) complex appeared at 520 nm, assignable to the $^4A_2g \rightarrow {}^4T_1g^{(P)}$ transition, indicating an octahedral coordination environment. The Co(II) complex assigned an absorption band at 894 nm, which belongs to $^4T_1g^{(F)} \rightarrow {}^4T_2g^{(F)}$ transition. This spectral information suggests a distorted six-coordinate geometry around the cobalt ion[36-39]. On the other hand, the Ni(II) complex reveals a band at 657 nm, relating to the $^3A_2g^{(F)} \rightarrow {}^3T_2g^{(F)}$ transition[40]. These results led to improving the distorted octahedral structure. Finally, the Cu(II) complex exhibited a band at 504 nm, attributed to the $^2B_1g \rightarrow {}^2A_2g$ transition[41,42]. These spectral findings indicate a tetrahedral geometry around the copper ion[43].

4.4. Thermal analysis

The TGA analysis of the ligand exhibited three distinct decomposition stages. The first stage, occurring between 100 and 180°C, accounted for approximately 30% of the mass loss and likely corresponds to the loss of adsorbed solvent or moisture beginning near 130°C, followed by cleavage of moieties consistent with CH_3OH + HCl near 180°C. The second stage, from about 210 to 330°C, produced a further 27% mass loss and is consistent with the evolution of volatile fragments such as butene and N_2. The final decomposition proceeded gradually up to 800°C, resulting in a remaining of 33% mass loss; the residual fragment is best represented by the empirical composition C_4H_5ClO; as seen in **Figure 4**. The TGA analysis of the Cu(II) complex was obtained. The Cu(II) complex thermogram showed four decomposition stages. The initial stage (120-180°C) involved a 20% mass loss attributed to the removal of adsorbed water and the decomposition of a labile organic fragment consistent with C_8H_9NO. The second stage, approximately at (180-270°C), accounted for an additional 20% mass loss, assignable to loss of a fragment matching $C_8H_{10}ClN$. The third and most extensive stage produced about 50% mass loss occurring around 270-800°C and corresponds to the breakdown of the principal organic framework, consistent with $C_{12}H_8Cl_5N_2O$. The remaining ~10% is attributed to the formation of the metal oxide residue, which lies near the instrument's detection limit, as shown in **Figure 5**.

5. Conclusion

The coupling reaction can be explained by the fact that the OH group is directed towards the *o*- and *p*- sites, and since one of the *o*- sites is actually occupied by chlorine and the *p*- site is also spatially restricted by a chlorine atom at the adjacent *m*- site, it is clear that the electrophile substitution is directed towards the remaining highly stable *o*- site. The synthesized azo dye (E)-1-[4-(3,4-dichloro-2-hydroxyphenyl)diazenyl]phenylethan-1-one was obtained in good purity and fully characterized, confirming its azo–phenolate structure and bidentate coordination ability. Spectroscopic and mass spectrometric data demonstrate coordination via phenolic and carbonyl oxygen atoms, while NMR and IR results verify the ligand's structural integrity and tautomeric behavior. Metal complexation with Cr(III), Co(II), Ni(II), and Cu(II) produced predominantly distorted octahedral geometries for the first four metals and a four-coordinate tetrahedral geometry for Cu(II), consistent with electronic and magnetic data. Thermal analysis indicates that both the ligand and its complexes exhibit multi-stage decomposition with substantial thermal stability and well-defined residues. The plane in which the acetophenone group is located is different from the plane in which the chlorinated phenol group is located, thus making the carbonyl and OH groups opposite each other. Furthermore, the axial rotation of the acetyl single bond on the plane of the acetophenone group reinforces the opposite relationship with the OH group. This helped position the metal opposite the carbonyl and hydroxide to coordinate with them; the spectral data supported this, whereas we ruled out association with the azo group because no change in its spectral properties was observed. The combined properties—tunability of coordination geometry, thermal robustness, and characteristic electronic transitions—make the ligand and its metal complexes promising candidates for a range of applications.

Acknowledgment

The authors thank the University of Baghdad, the College of Education for Pure Science (Ibn Al-Haitham), and the Department of Chemistry for their assistance in facilitating the researchers' activities.

Conflict of Interest

The authors declared that they have no competing interests.

Funding

Non applicable.

References

1. Saini R, Choudhary K. Toxic potential of azo dyes: A broader understanding. In: Hazardous Chemicals. Elsevier; 2025. p. 469–481. https://doi.org/10.1016/B978-0-323-95235-4.00039-6.
2. Antonov L. Tautomerism in azo and azomethyne dyes: When and if theory meets experiment. Molecules. 2019; 24(12):2252. https://doi.org/10.3390/molecules24122252.
3. Hajra C, Datta A. Substitutional control of non-statistical dynamics in the thermal deazetization of tetracyclic azo compounds. Phys Chem Chem Phys. 2024; 26(44):28161–28170. https://doi.org/10.1039/D4CP03447C.
4. Tripathy L, Sarangi AK. Synthesis, characterization, biological and computational insights of some binuclear azo dye-based metal complexes. Appl Organomet Chem. 2025; 39(11):e70407. https://doi.org/10.1002/aoc.70407.
5. Li S, Zhao W, Qi Y, Niu W, Ma W, Tang B, Zhang S. Hydrogen bonding induced ultra-highly thermal stability of azo dyes for color films. Chinese Chem Lett. 2025; 36(9):110653. https://doi.org/10.1016/j.cclet.2024.110653.
6. Deivayanai VC, Karishma S, Thamarai P, Saravanan A, Yaashikaa PR. Efficient red azo dye removal from wastewater using magnetic nanoparticle impregnated Prosopis juliflora biomass: ANN modeling approach. Desalin Water Treat. 2024; 320:100746. https://doi.org/10.1016/j.dwt.2024.100746.

7. Haque T, Shompa MA, Khayer K. DFT study of structural, electronic, and charge-transfer properties of 2-naphthol azo derivatives: Geometric, positional, and substituent effects. J Phys Chem A. 2025; 129(5): 1252–1279. https://doi.org/10.1021/acs.jpca.4c06467.
8. Brillas E, Oliver R. Development of persulfate-based advanced oxidation processes to remove synthetic azo dyes from aqueous matrices. Chemosphere. 2024;355:141766. https://doi.org/10.1016/j.chemosphere.2024.141766.
9. Sharma M, Sharma S, Alkhanjaf AAM, Arora NK, Saxena B, Umar A, Ibrahim AA, Akhtar MS, Mahajana AM, Negi S, Kumar A, Baskoutas S. Microbial fuel cells for azo dye degradation: A perspective review. J Ind Eng Chem. 2025;142(10):45–67. https://doi.org/10.1016/j.jiec.2024.07.031.
10. Khan MN, Parmar DK, Das D. Recent applications of azo dyes: A paradigm shift from medicinal chemistry to biomedical sciences. Mini Rev Med Chem. 2021; 21(9):1071–1084. https://doi.org/10.2174/1389557520999201123210025.
11. Rodríguez-Vargas JA, Díaz-Rodríguez SH, Vergara-Rodríguez VG, Vidal-Rosado Á, Rivera-Torres C, Ríos-Rodríguez A, Valle R-D, Agosto-Disdier MD, Torres-Díaz M, Griebenow KH, Rodríguez-Berríos RR. Synthesis, purification, characterization, and ABTS antioxidant evaluation of novel azo dyes. Organics. 2025; 6(3):39. https://doi.org/10.3390/org6030039.
12. Unnisa A, Abouzied AS, Baratam A, Lakshmi KNVC, Hussain T, Kunduru RD, Banu H, Fatima SB, Hussian A, Selvarajan KK. Design, synthesis, characterization, computational study and in-vitro antioxidant and anti-inflammatory activities of few novel 6-aryl substituted pyrimidine azo dyes. Arab J Chem. 2020; 13(12):8638–8649. https://doi.org/10.1016/j.arabjc.2020.09.050.
13. da Rocha JR, Alcântara MGDS, Silva VFN, Paz Lima DJD, Santos JCC. Acid phosphatase detection using a colorimetric probe based on azo compound toward forensic applications for seminal fluid identification. Dye Pigment. 2025; 239:112806. https://doi.org/10.1016/j.dyepig.2025.112806.
14. Rahman M, Tabassum Z. Biotechnological approach to treat textile dyeing effluents: A critical review analysing the practical applications. Text Leather Rev. 2024; 7:125–152. https://doi.org/10.31881/TLR.2023.189.
15. El-Sayed E, Abd El-Aziz E, Othman H, Hassabo A. Azo dyes: Synthesis, classification and utilisation in textile industry. Egypt J Chem. 2024. https://doi.org/10.21608/ejchem.2024.257952.9057.
16. Moorchilot VS, Aravind UK, Aravindakumar CT. Occurrence of azo-dyes, plasticizers, and PAH-bound microplastics: an emerging source and sink for hazardous compounds in indoor environments? Air Qual Atmos Heal. 2024; 17(2):425–438. https://doi.org/10.1007/s11869-023-01455-5.
17. Desai KKB, Badgujar NP, Vishnu S, Thakor K, Nagaraj K. Co-diazotization-based structural modification of azo pigments: enhanced coloristic properties of pigment red pigments for industrial ink applications. J Indian Chem Soc. 2025; 102(9):101979. https://doi.org/10.1016/j.jics.2025.101979.
18. Mezher MQ, Yousif EI. Synthesis, spectral characterisation and biological evaluation of a new azo-ligand derived from a minoacetophenone with its metal complexes. ICAIIT. 2025; 13(2):623–633. http://dx.doi.org/10.25673/120550.
19. Jarad AJ, Dahi MA, Al-Noor TH, El‑ajaily MM, AL-Ayash SR, Abdou A. Synthesis, spectral studies, DFT, biological evaluation, molecular docking and dyeing performance of 1-(4-((2-amino-5-methoxy) diazenyl) phenyl) ethanone complexes with some metallic ions. J Mol Struct. 2023; 1287:135703. https://doi.org/10.1016/j.molstruc.2023.135703.
20. Shukla AK, editor. Advances in spectroscopic analysis of food and drink. IOP Publishing; 2024; 2053-2563. https://doi.org/10.1088/978-0-7503-5573-510.1088/978-0-7503-5573-5.
21. Rezaeianzadeh O, Asghari S, Tajbakhsh M, Mohseni M, Khalilpour A. Synthesis, molecular docking, and anticancer evaluation of new azo-based sulfonamides against MCF-7 human breast cancer cell line. Chem Methodol. 2024; 8(5):329–350. https://doi.org/10.48309/CHEMM.2024.447205.1773.
22. Hussain SA, Al-Jeboori MJ. New metal complexes derived from Mannich-base ligand; synthesis, spectral characterisation and biological activity. J Glob Pharma Tech. 2019; 11(2):548–560.
23. Abraham RJ, Mobli M. An NMR, IR and theoretical investigation of ^{1}H chemical shifts and hydrogen bonding in phenols. Magn Reson Chem. 2007; 45(10):865–877. https://doi.org/10.1002/mrc.2060.
24. Gunawan R, Nandiyanto ABD. How to read and interpret ^{1}H-NMR and ^{13}C-NMR spectrums. Indones J Sci Technol. 2021; 6(2):267–298. https://doi.org/10.17509/ijost.v6i2.34189.
25. Olakojo OO, Beitz E, Girreser U, Adegoke AO, Idowu SO. Spectroscopic investigation of azo-hydrazo tautomerization in naphthalene-based azo dyes using 1D and 2D NMR. J Chem Sci. 2025; 137(4):1–15. https://doi.org/10.1007/s12039-025-02425-3.

26. Hillel C, Collins S, Parihar A, Mermut O, Barrett CJ, Pietro WJ, Reven L. Solid state NMR and DFT studies of azo–hydrazone tautomerism in azo dyes and chitosan-dye films. Phys Chem Chem Phys. 2025; 27(10):5228–5237. https://doi.org/10.1039/D4CP04159C.
27. Silverstein RM, Bassler GC. Spectrometric identification of organic compounds. J Chem Educ. 1962; 39(11):546. https://doi.org/10.1021/ed039p54610.1021/ed039p546.
28. Smejkalova D, Spaccini R, Fontaine B, Piccolo A. Binding of phenol and differently halogenated phenols to dissolved humic matter as measured by NMR spectroscopy. Environ Sci Technol. 2009; 43(14):5377–5382. https://doi.org/10.1021/es900559b.
29. Agrawal PK, Blunden G. Methoxy ^{13}C NMR chemical shift as a molecular descriptor in the structural analysis of flavonoids and other phenolic compounds. Nat Prod Commun. 2023; 18(6):1-6. https://doi.org/10.1177/1934578X231171002.
30. Kruve A, Kaupmees K. Adduct formation in ESI/MS by mobile phase additives. J Am Soc Mass Spectrom. 2017; 28(5):887–894. https://doi.org/10.1007/s13361-017-1626-y10.1007/s13361-017-1626-y.
31. Aghara RV, Parmar MC, Patel BY. Synthesis of pyridine clubbed tetrahydrobenzo [b] thiophene azo dye analogues using the gewald reaction: Catalytic optimization, antibacterial, and dye investigation. Russ J Gen Chem. 2023; 93(9):2393–2403. https://doi.org/10.1134/S1070363223090207.
32. Haslam E. Protection of phenols and catechols. In: Protective Groups in Organic Chemistry. Springer; 1973, p. 145–182.
33. Ashenhurst JA. Synthetic studies on the phomoidrides. McGill University; 2006. https://escholarship.mcgill.ca/concern/theses/ns064990s.
34. Lever ABP. Electronic spectra of dn ions. Inorg Electron Spectrosc. 1984; 2:376–611. http://dx.doi.org/10.4236/ns.2010.29127.
35. Ovung A, Bhattacharyya J. Sulfonamide drugs: Structure, antibacterial property, toxicity, and biophysical interactions. Biophys Rev. 2021; 13(2):259–272.https://doi.org/10.1007/s12551-021-00795-9.
36. Yousef TA, Abu El-Reash GM, Abu AL-Zahab M, Safaan MAA. Physicochemical investigations, biological studies of the Cr(III), Mn(II), Fe(III), Co(II), Ni(II), Cu(II), Zn(II), Cd(II), Hg(II) and UO2(VI) complexes of picolinic acid hydrazide derivative: A combined experimental and computational approach. J Mol Struct. 2019; 1197:564–575. https://doi.org/10.1016/j.molstruc.2019.07.088.
37. Fnfoon DY, Al-Adilee KJ. Synthesis and spectral characterization of some metal complexes with new heterocyclic azo imidazole dye ligand and study biological activity as anticancer. J Mol Struct. 2023; 1271:134089. https://doi.org/10.1016/j.molstruc.2022.134089.
38. Ramachandran E, Gandin V, Bertani R, Sgarbossa P, Natarajan K, Bhuvanesh NSP, Venzo A, Zoleo A, Glisenti A, Dolmella A, Albinati A, Marzano C. Synthesis, characterization and cytotoxic activity of novel copper (II) complexes with aroylhydrazone derivatives of 2-Oxo-1, 2-dihydrobenzo [h] quinoline-3-carbaldehyde. J Inorg Biochem. 2018; 182:18–28. https://doi.org/10.1016/j.jinorgbio.2018.01.016.
39. Singh R V, Dwivedi R, Joshi SC. Synthetic, magnetic, spectral, antimicrobial and antifertility studies of dioxomolybdenum (VI) unsymmetrical imine complexes having a N∩ N donor system. Transit Met Chem. 2004; 29(1):70–74. https://doi.org/10.1023/B:TMCH.0000014487.86754.93.
40. Derafa WM, Elkanzi NAA, Ali AM, Abdou A. Three Co (II), Ni (II) and Cu (II) Schiff base complexes incorporating 2-[(4-{[(4-methylphenyl) sulfonothioyl] oxy} phenyl) methylene] amino} benzoic acid: Synthesis, structural, dft, biological and molecular docking investigation. Bull Chem Soc Ethiop. 2024; 38(2):325–346. https://doi.org/10.4314/bcse.v38i2.5.
41. Athuiny AA. Spectral and physical studying of dithiocarbamate mixed ligand complexes. Iraqi J Sci Ind Res. 2025; 4(3):86–90. http://ijsir.com/index.php/ijsir/article/view/95
42. Ngo ACR, Tischler D. Microbial degradation of azo dyes: approaches and prospects for a hazard-free conversion by microorganisms. Int J Environ Res Public Health. 2022; 19(8):4740. https://doi.org/10.3390/ijerph19084740.
43. Hulankova R. Methods for determination of antimicrobial activity of essential oils in vitro—A Review. Plants. 2024; 13(19):2784. https://doi.org/10.3390/plants13192784.